

Synthesis and Characterization of $\text{La}_{1-x}\text{Sr}_x\text{MnO}_{3\pm\delta}$ Powders Obtained by the Polymeric Precursor Route

Adriano Alves Rabelo^{a*}, Marfran Cardoso de Macedo^b, Dulce Maria de Araújo Melo^b,

Carlos Alberto Paskocimas^b, Antonio Eduardo Martinelli^b, Rubens Maribondo do Nascimento^b

^aFaculty of Materials Engineering, Federal University of Pará,

Folha 17, Quadra 04, Lote Especial, CEP 68505-080, Marabá, PA, Brazil

^bFederal University of Rio Grande do Norte, P.O. Box 1662, CEP 59072-970, Natal, RN, Brazil

Received: November 26, 2010; Revised: February 25, 2011

Polycrystalline strontium-doped lanthanum manganite (LSM) powders with 0.15, 0.22, and 0.30 mol % Sr were synthesized by the polymeric precursor route using a molar ratio of 3:1 citric acid and metal cations. The powders were characterized by Fourier transform infrared spectroscopy, thermal analysis, high-temperature X-ray diffraction to determine the crystalline perovskite phase and crystallite sizes, scanning electron microscopy for the morphological analysis, nitrogen adsorption to determine the specific surface area, and laser scattering to evaluate the particle size distribution. The LSM perovskite-type oxides containing intermediate 0.22 mol % Sr were found to exhibit a tendency to decrease in crystallite size and increase in specific surface area and, when calcined at 700–900 °C exhibited a pure phase of perovskite, had a crystallite size of about 17–20 nm and a specific surface area for 900 °C of 34.3 m².g⁻¹.

Keywords: perovskite, polymeric precursor, SOFC

1. Introduction

Strontium-doped lanthanum manganite perovskite oxides ($\text{La}_{1-x}\text{Sr}_x\text{MnO}_{3\pm\delta}$, LSM) have been widely studied in recent years due to their interesting applications in solid oxide fuel cells (SOFC), oxi-reduction catalysts (automotive catalysis), sensors and memories¹⁻⁶. These latter applications are due to the outstanding magnetotransport properties of these oxides⁷⁻⁹. In the LSM perovskite structure, Mn³⁺ or Mn⁴⁺ ions are the network formers, occupying the octahedral B sites and are associated to the oxygen reduction, whilst the ion La³⁺, partially replaced in the twelve-fold oxygen coordinated sites A, are related to the property of electronic conduction. The intrinsic properties of these materials can be affected by small network distortions (stoichiometry), by the crystallite size, specific surface area and working temperature^{10,11}. The LSM oxides as the cathode have proved to be very poor oxide ion conductors, but their electronic conductivity is high enough to make them attractive SOFC cathode material, which is particularly interesting when the strontium content is 0.1 to 0.3. The $\text{La}_{0.8}\text{Sr}_{0.2}\text{MnO}_3$ gives a good combination of electronic conductivity and expansion coefficient matching, and is now available commercially for SOFC applications. Higher conductivity can be obtained at higher dopant levels, but the expansion coefficient then becomes too high¹²⁻²⁰.

There are several routes to synthesize perovskite structured materials. These routes include the polymeric precursor route or the Pechini method²¹⁻²³, which stands out for its enhanced stoichiometric control, allowing for doping in a ppm order of magnitude, with good composition homogeneity, depending on the system's composition. This method also allows one to obtain relatively high specific surface area powders when compared with other traditional solid state reaction methods²⁴⁻²⁶.

The key point of this route is to obtain a polymeric precursor resin, a branched chain polymer, in which the cations are distributed randomly. The method involves the complexation reactions of citric acid with the metal ions and polyesterification with ethylene glycol. The progressive heating in air up to around 95 °C promotes the

condensation reaction with the formation of water molecules. At this temperature the polyesterification reaction takes place and excess water is eliminated, resulting in a polymeric resin from which the powder is obtained. In the present work, the polymeric precursor method was used to prepare strontium-doped lanthanum manganite, $\text{La}_{1-x}\text{Sr}_x\text{MnO}_3$, where $x = 0.15, 0.22$ and 0.30 , with the purpose of obtaining powders with high specific surface areas.

2. Experimental

2.1. Chemical synthesis

The $\text{La}_{1-x}\text{Sr}_x\text{MnO}_3$ samples were synthesized by the polymeric precursor route, based in Pechini method, which has been used to synthesize polycation oxides. The starting materials were lanthanum nitrate (>99.0%, Vetec), strontium nitrate (>99.0%, Vetec), manganese nitrate (>97.0%, Vetec), citric acid (>99.0%, Chromato), ethylene glycol (>99.5%, Vetec) and distilled water. The concentrations of nitrate solutions were previously determined by gravimetry.

Manganese citrate solution was prepared from $\text{Mn}(\text{NO}_3)_2 \cdot 4\text{H}_2\text{O}$ and citric acid, using the citric acid/metal cation molar ratio of 3:1, under stirring at 70 °C for 2 hours. The network modifier and the dopant were later added. The resulting solution was subjected to mechanical stirring and heating at 90 °C. Afterwards ethylene glycol was added at a 60:40 citric acid/ethylene glycol mass ratio.

This solution was kept at mechanical agitation and heating at 95 °C for 2 hours to form the polymeric resin, which was later heat-treated at 300 °C for 2 hours, yielding a fragile and porous solid. Such material was initially disaggregated in a mortar and later ground for 2 hours in a planetary mill (Pulverisette 2000, Fritsch). Subsequently, the powders were calcined at 450, 700 and 950 °C for 4 hours at a heating rate of 5 °C/min. The heat-treated powders were again dried and disaggregated in the planetary mill down to a mesh size of less than 200 in a Tyler sieve.

*e-mail: adrianoalves@ufpa.br

2.2. Characterization methods

The heat-treated powders were subjected to Fourier transform infrared spectroscopy analyses (FTIR, Perkin-Elmer/16PC), in a range of 500 to 4000 cm^{-1} . The TG/DTG (Shimadzu/TGA-50H) curves for the samples synthesized and pre-calcined powders at 300 °C for 2 hours were obtained in air, at a heating rate of 10 °C/min, up to 1000 °C. The average crystallite sizes and the constituent phases were determined by high-temperature X-ray diffraction, using the $\text{Cu-K}\alpha$ radiation at a step of 0.02°/s with $2\theta = 10$ to 60° (Shimadzu/XRD-6000 diffractometer). Scherrer's equation was used to calculate the average crystallite size (t), adopting an average of the five most intense XRD peaks, as follows:

$$t = \frac{\kappa\lambda}{\beta\cos\theta} \quad (1)$$

where κ is a constant equal to 0.9; λ is the X-ray wavelength, and β is the full width at half-maximum of the X-ray reflection.

The average particle sizes (d_{50}) of powders were obtained by laser scattering (CILAS/1064) in distilled water with an ultrasonic treatment for 120 seconds. The wide of distribution particle sizes was analyzed using the values of the relation d_{90}/d_{50} .

The specific surface area (S_{BET}) values were determined by the BET method (Nova 2000, Quanta-Chrome) in five points of linear region in the adsorption isotherm. The average pore size (D_p) was calculated by the BJH method²⁷. The equivalent spherical diameter, d_{BET} was calculated by Equation 2, in which d_{BET} is the equivalent spherical diameter, S_{BET} is the specific surface area ($\text{m}^2\cdot\text{g}^{-1}$) and ρ is the theoretical phase density. The adopted density values were 6.6 $\text{g}\cdot\text{cm}^{-3}$ for $\text{La}_{0.85}\text{Sr}_{0.15}\text{MnO}_3$, 6.5 $\text{g}\cdot\text{cm}^{-3}$ for $\text{La}_{0.78}\text{Sr}_{0.22}\text{MnO}_3$ and 6.4 $\text{g}\cdot\text{cm}^{-3}$ for $\text{La}_{0.70}\text{Sr}_{0.30}\text{MnO}_3$.

$$d_{\text{BET}} = \frac{6}{S_{\text{BET}}\rho} \quad (2)$$

The morphology of the powders was analyzed by scanning electron microscopy (SEM, Philips/XL-30 FEG).

Apparent density (% of theoretical density) measurements were taken by the Archimedes method, using samples pressed at 37 MPa and sintered at 1350 °C for 4 hours in air (Jung/2314 furnace).

3. Results and Discussion

Figure 1 shows the infrared spectra of the synthesized $\text{La}_{1-x}\text{Sr}_x\text{MnO}_3$ precursor powders ($x = 0.15, 0.22$ and 0.30) heat-treated at 450 °C for 4 hours. The broad band in the region of 3500 cm^{-1} is related to the O-H group, which is associated to citrates and/or water molecules coordinated with the metal ions. The band positioned between 3200 and 2500 cm^{-1} was referred to the intramolecular hydrogen with C=O bond. A band observed at 1750 cm^{-1} is related to the C=O bond of acid with axial deformation. The bands observed between 1546 and 1362 cm^{-1} are ascribed to the stretching vibrations of the carboxylate (COO) groups, or C-H bonds. At 1000 cm^{-1} , the band observed was referred to C-O bond from esters²⁸. It was observed for the strontium doping sample with $x = 0.15$ a strong band related to metal-oxygen bond at 600 cm^{-1} , indicating the formation of the respective oxide.

For the synthesized precursor powders heat-treated at 700 °C for 4 hours (Figure 2), only the strontium-doped sample with $x = 0.22$ showed the band related to O-H bond, in the region of 3500 cm^{-1} . This same composition showed a band related to the metal-oxygen bond at 600 cm^{-1} , indicating the formation of the respective oxide. The remaining absorption bands were similar to the ones described for the samples calcined at 450 °C.

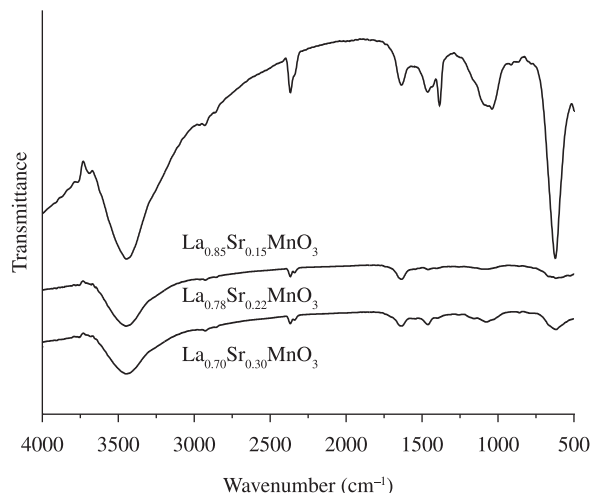


Figure 1. FTIR absorption patterns of $\text{La}_{0.85}\text{Sr}_{0.15}\text{MnO}_3$, $\text{La}_{0.78}\text{Sr}_{0.22}\text{MnO}_3$ and $\text{La}_{0.70}\text{Sr}_{0.30}\text{MnO}_3$ powders, calcined at 450 °C for 4 hours.

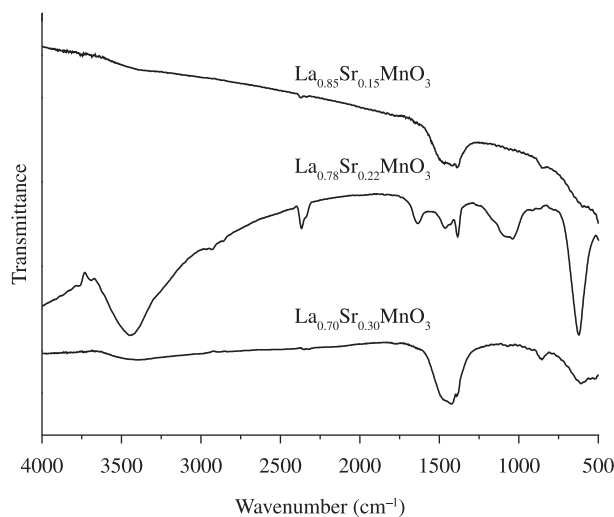


Figure 2. FTIR absorption patterns of $\text{La}_{0.85}\text{Sr}_{0.15}\text{MnO}_3$, $\text{La}_{0.78}\text{Sr}_{0.22}\text{MnO}_3$ and $\text{La}_{0.70}\text{Sr}_{0.30}\text{MnO}_3$ powders calcined at 700 °C for 4 hours.

When the precursor powder was heat-treated at 950 °C for 4 hours, the spectrum did not show any characteristic band of organic compounds in a range from 4000 to 500 cm^{-1} , as depicted in Figure 3. Accordingly, the band observed at 600 cm^{-1} , which was ascribed to the metal-oxygen bond, indicates the formation of the corresponding oxides.

The thermogravimetric and differential thermogravimetric (TG/DTG) analyses of $\text{La}_{0.85}\text{Sr}_{0.15}\text{MnO}_3$ precursor powder are shown in Figure 4. The first stage of thermal decomposition from 30 to 200 °C was related to the elimination of water, derived from the esterification reaction, and from ethylene glycol excess. The second stage, from 300 to 570 °C, corresponded to the breakage of the polymeric chain formed by the polyesterification, whereas the third thermal decomposition stage, from 600 to 820 °C, was ascribed to decomposition of the remaining organic compounds. For higher temperatures, mass losses associated to organic compounds were no longer detected. The overall mass loss was approximately 12%. For temperatures as higher as 830 °C the material became stable in terms of mass loss, with only the formation of the oxide.

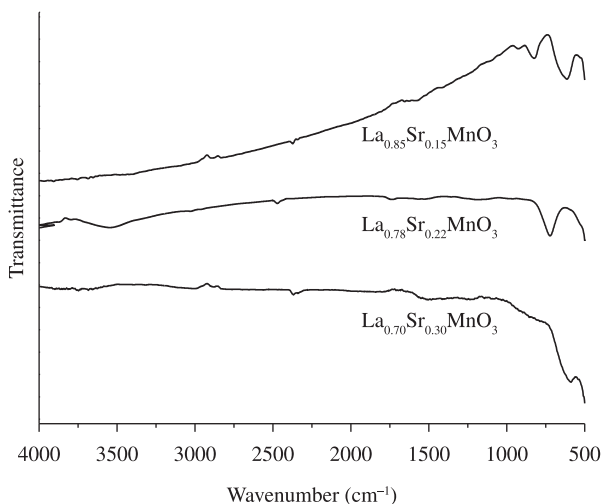


Figure 3. FTIR absorption patterns of $\text{La}_{0.85}\text{Sr}_{0.15}\text{MnO}_3$, $\text{La}_{0.78}\text{Sr}_{0.22}\text{MnO}_3$ and $\text{La}_{0.70}\text{Sr}_{0.30}\text{MnO}_3$ powders calcined at 950 °C for 4 hours.

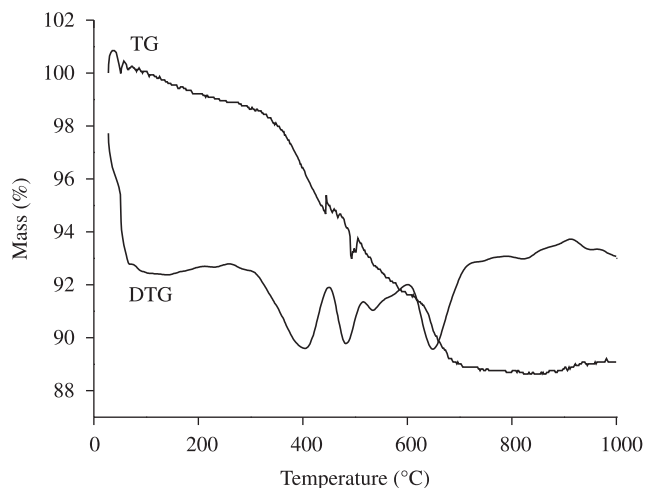


Figure 5. Thermogravimetric and differential thermogravimetric analyses of $\text{La}_{0.78}\text{Sr}_{0.22}\text{MnO}_3$ precursor powder.

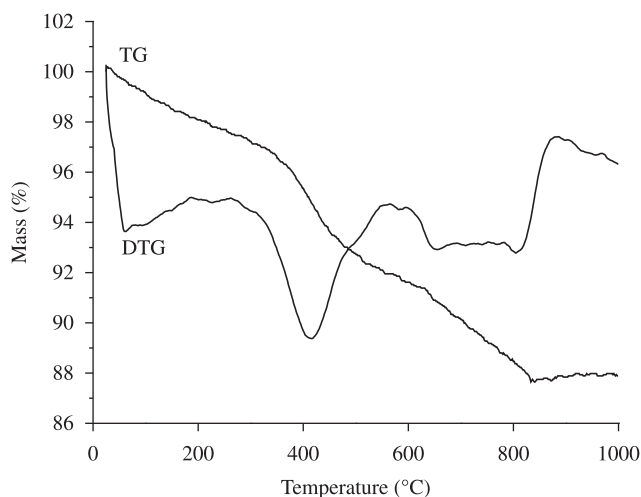


Figure 4. Thermogravimetric and differential thermogravimetric analyses of $\text{La}_{0.85}\text{Sr}_{0.15}\text{MnO}_3$ precursor powder.

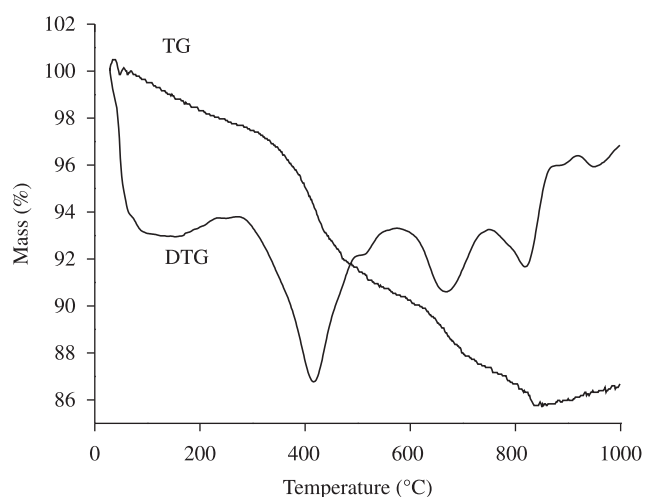


Figure 6. Thermogravimetric and differential thermogravimetric analyses of $\text{La}_{0.70}\text{Sr}_{0.30}\text{MnO}_3$ precursor powder.

The thermal decomposition process of $\text{La}_{0.78}\text{Sr}_{0.22}\text{MnO}_3$ took place in five steps, according to Figure 5. The overall mass loss was 11%, which occurred between 30 and 750 °C. The first thermal decomposition stage, from 30 to 200 °C, was attributed to the exit of water molecules associated to the organic matter. In the second and third steps the polymer decomposition took place, characterized by an abrupt mass loss at approximately 500 °C, whereas in the subsequent steps from 600 to 760 °C, the mass loss was attributed to the decomposition of carbonaceous materials. After these events, only formation of the respective oxide occurred at a temperature of about 880 °C.

The TG/DTG curves of the sample $\text{La}_{0.70}\text{Sr}_{0.30}\text{MnO}_3$ are depicted in Figure 6 and presented a thermal behavior similar to the ones of the samples $\text{La}_{0.85}\text{Sr}_{0.15}\text{MnO}_3$ and $\text{La}_{0.78}\text{Sr}_{0.22}\text{MnO}_3$. The overall mass loss was 14%, most of it associated to decomposition of the organic matter. The first stage from 30 to 200 °C referred to the exit of water, either from the polyesterification reaction or coordination water. The second stage, from 300 to 570 °C, corresponded to the breakage of the polymer chain formed by the polyesterification reaction and the third and the fourth stages, from 600 to 820 °C, referred to

decomposition of organic compounds. Sample mass increased at temperatures exceeding approximately 850 °C owing to oxidation of the material. With regard to the higher mass loss of $\text{La}_{0.70}\text{Sr}_{0.30}\text{MnO}_3$ powder precursor, it is probably attributable to the higher content of strontium, which was added in the form of nitrate.

By the thermal analyses of the three compositions synthesized in this work, it was possible to observe a small mass gain from about 820 °C, which was associated to oxidation of lanthanum manganite and strontium manganite in the perovskite structure, due to the variation of oxidation state of manganese cation. For the case of 22% strontium doping, in which the mass loss is finished at a temperature lower than the case of the remaining doping levels, this oxidation also took place.

The evolution of the crystalline phase with increasing temperature at the three levels of doping, which was observed by high-temperature XRD, is illustrated in Figures 7, 8 and 9. The XRD patterns indicated that the formation of the perovskite structure of $\text{La}_{1-x}\text{Sr}_x\text{MnO}_3$ was completed at a temperature of 600 °C. The occurrence of secondary phases was attributed to oxidation of Mn cations on the surface. A decomposition of manganite phases above 900 °C is a possible

immiscibility gap of the perovskite, lanthanum manganite and strontium manganite phases at high temperatures, which was more evident with larger amounts of strontium.

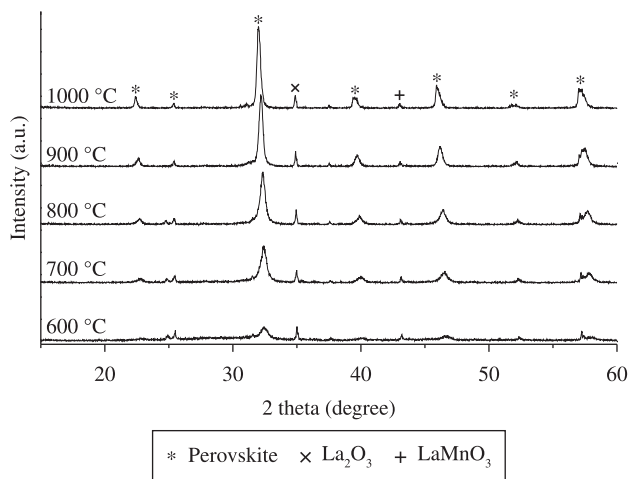


Figure 7. High temperature XRD patterns of $\text{La}_{0.85}\text{Sr}_{0.15}\text{MnO}_3$.

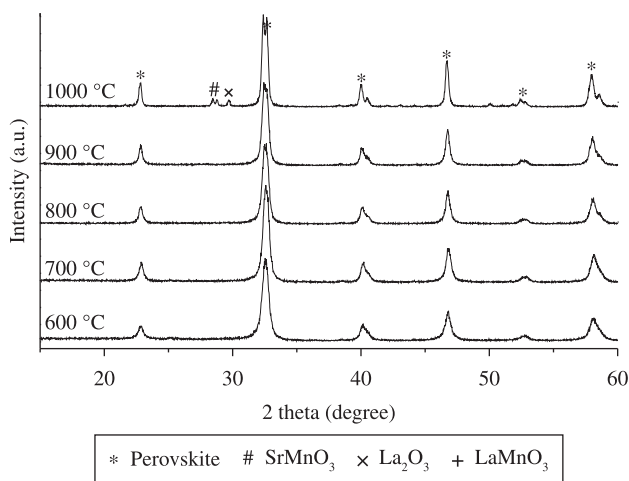


Figure 8. High temperature XRD patterns of $\text{La}_{0.78}\text{Sr}_{0.22}\text{MnO}_3$.

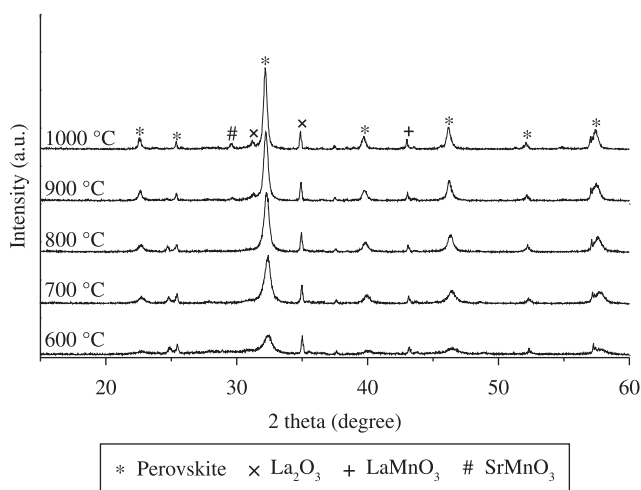


Figure 9. High temperature XRD patterns of $\text{La}_{0.70}\text{Sr}_{0.30}\text{MnO}_3$.

Analyzing the average crystallite sizes obtained at different temperatures (Table 1), it can be noticed that the LSM perovskite-type oxides containing the intermediate 22% strontium showed a tendency to decrease the crystalline size and increase the specific surface area (Table 2). This result was not in agreement with that verified for $\text{La}_x\text{Sr}_{1-x}\text{FeO}_3$ ^[29] and $\text{La}_{1-x}\text{Sr}_x\text{CoO}_3$ perovskites³⁰ in which a size increase, associated to the increase of doping level took place. This can be attributed to the change of orthorhombic phase, for 10% of strontium, to rhombohedral phase for 22% or more of strontium. Substitution of La with lower valence cations (such as Sr^{2+} and Ca^{2+}) or A-site deficiency increases the concentration of Mn^{4+} in the LaMnO_3 lattice. This eventually decreases the orthorhombic to rhombohedral (> 600 °C) transformation temperature.

The XRD patterns of the specimens calcined demonstrated the existence of a structure of which was identified as perovskite-type in all the compositions. The lattice parameter of each sample was obtained considering JCPDS information card (N° 35-1353) existing of undoped lanthanum manganites material, which it allowed to find the lattice parameters at 800 °C. The identification was of visual and comparative character. The lattice parameter decreases with increasing Sr^{2+} concentration from 5.5318 to 5.4960 Å when the doping level changes from 0.15 to 0.22 mol %, and then increases again with addition of 0.30 mol % to 5.5391 Å. Since the ionic radii of Sr^{2+} and La^{3+} are 1.44 and 1.36 Å respectively³¹, there is a substitutional solid solution as the La^{3+} was replaced by the larger Sr^{2+} cation, which presents the largest ray, limiting the substitution of the La^{3+} by the Sr^{2+} in the LaMnO_3 perovskite-type structure. When two moles of SrO dissolves into LaMnO_3 , there form a negative charged divalent substituted strontium site and a positive charged divalent oxygen vacancy. And it is implied by the lattice parameter that the perovskite-type changes from orthorhombic distortion to rhombohedral when the doping level was greater than 0.22 mol %. The nonlinear variation of the lattice parameter is attributed to this phase change.

Table 2 shows the values of specific surface area, equivalent the spherical diameter, average particle size and average pore diameter, determined for the three doping levels of $\text{La}_{1-x}\text{Sr}_x\text{MnO}_3$ system, for different heat treatment temperatures studied in this work, as well as the apparent density after sintering at 1350 °C for 4 hours.

The average crystallite size was in the range of 20 nm. The average particle size (d_{50}) for the powders heat-treated at 450, 700 and 950 °C for 4 hours revealed the presence of agglomerates, since approximately 100-fold higher values were obtained, as well as the width of the distribution (D_{90}/D_{50}), which was very wide for all the powders. The wide particle size distribution, allied to the presence of agglomerates, contributed to the formation of density gradients, thus generating internal stresses in the pressed bodies.

The average pore diameter indicated that the powders were in the inferior region of porosity, classified as mesoporous (200-500 nm). The apparent density after sintering at 1350 °C for 4 hours was in the range from approximately 70 to 80% of the theoretical density in these conditions. These physical characteristics indicate possible applications such as in solid oxide fuel cells or in catalysis.

Table 1. Average crystallite size (nm) of $\text{La}_{0.85}\text{Sr}_{0.15}\text{MnO}_3$, $\text{La}_{0.78}\text{Sr}_{0.22}\text{MnO}_3$ and $\text{La}_{0.70}\text{Sr}_{0.30}\text{MnO}_3$ from 600 to 1000 °C.

Sample / temperature	600 °C	700 °C	800 °C	900 °C	1000 °C
$\text{La}_{0.85}\text{Sr}_{0.15}\text{MnO}_3$	17.0	20.1	23.4	24.7	31.2
$\text{La}_{0.78}\text{Sr}_{0.22}\text{MnO}_3$	15.1	16.8	18.4	19.8	23.4
$\text{La}_{0.70}\text{Sr}_{0.30}\text{MnO}_3$	18.2	22.9	24.0	25.0	34.8

Table 2. Results of specific surface area (S_{BET}), equivalent spherical diameter (d_{BET}), average particle size (d_{50}), width of particle size distribution (D_{90}/D_{50}) and average pore diameter (Dp) for $\text{La}_{0.85}\text{Sr}_{0.15}\text{MnO}_3$, $\text{La}_{0.78}\text{Sr}_{0.22}\text{MnO}_3$ and $\text{La}_{0.70}\text{Sr}_{0.30}\text{MnO}_3$ calcined at different temperatures (T) and apparent density (ρ_a), after sintering at 1350 °C/4 hours.

Sample	T (°C)	S_{BET} ($\text{m}^2\cdot\text{g}^{-1}$)	d_{BET} (nm)	d_{50} (μm)	d_{90}/d_{50}	Dp (nm)	ρ_a (%TD)
$\text{La}_{0.85}\text{Sr}_{0.15}\text{MnO}_3$	450	30.6	29.7	1.4	4.2	545	75.9
$\text{La}_{0.78}\text{Sr}_{0.22}\text{MnO}_3$	450	103.6	8.9	2.1	6.1	446	73.0
$\text{La}_{0.70}\text{Sr}_{0.30}\text{MnO}_3$	450	25.9	36.2	2.3	3.6	513	79.5
$\text{La}_{0.85}\text{Sr}_{0.15}\text{MnO}_3$	700	26.7	34.0	1.0	2.6	294	76.1
$\text{La}_{0.78}\text{Sr}_{0.22}\text{MnO}_3$	700	57.5	16.1	1.8	3.1	448	74.3
$\text{La}_{0.70}\text{Sr}_{0.30}\text{MnO}_3$	700	58.6	16.0	1.3	2.7	339	82.4
$\text{La}_{0.85}\text{Sr}_{0.15}\text{MnO}_3$	900	19.6	46.4	4.4	2.3	399	77.2
$\text{La}_{0.78}\text{Sr}_{0.22}\text{MnO}_3$	900	34.3	26.9	2.1	9.1	425	76.3
$\text{La}_{0.70}\text{Sr}_{0.30}\text{MnO}_3$	900	14.0	67.0	2.3	3.6	412	83.9

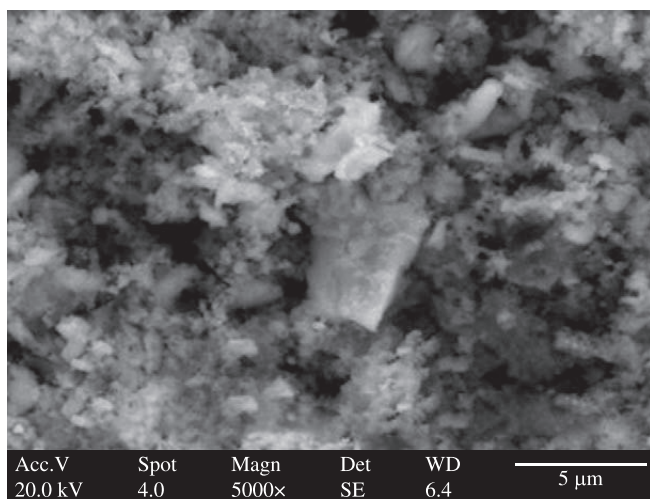


Figure 10. SEM micrograph of $\text{La}_{0.85}\text{Sr}_{0.15}\text{MnO}_3$ calcined at 450 °C/4 hours.

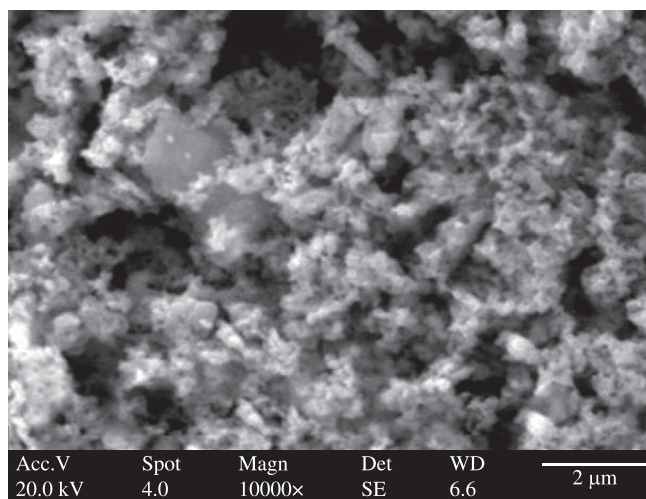


Figure 12. SEM micrograph of $\text{La}_{0.70}\text{Sr}_{0.30}\text{MnO}_3$ calcined at 450 °C/4 hours.

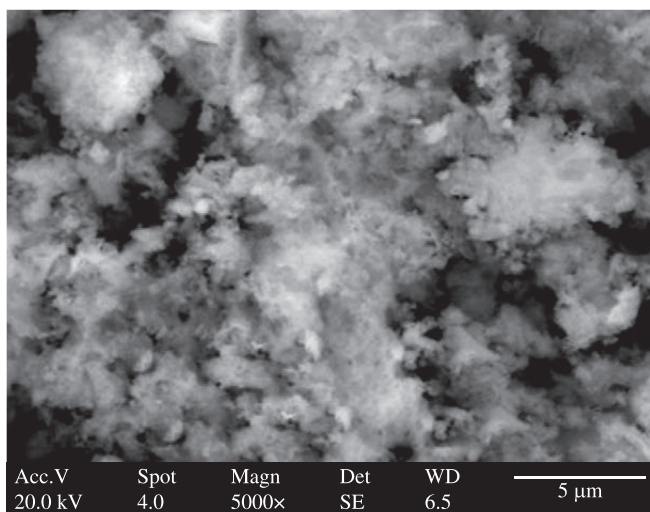


Figure 11. SEM micrograph of $\text{La}_{0.85}\text{Sr}_{0.15}\text{MnO}_3$ calcined at 950 °C/4 hours.

It has been reported a value of $20.2 \text{ m}^2\cdot\text{g}^{-1}$ for the specific surface area of $\text{La}_{1-x}\text{Mn}_x\text{MnO}_3$ ^[8], synthesized by the polymeric precursor method, when heat-treated at 700 °C for 6 hours. When the synthesis was carried out by the co-precipitation method, the specific surface area value obtained was only $8.3 \text{ m}^2\cdot\text{g}^{-1}$. Accordingly²⁶, it was reported a comparison between the different specific surface area values for strontium-doped lanthanum manganite obtained from different sources, carbonates, oxalates and citrates, in which the highest specific surface area value, $30 \text{ m}^2\cdot\text{g}^{-1}$, was obtained for the synthesis starting from citrates. Some disparity in values is due to a fluctuation in the texture of the particles, showing morphologies with different degrees of agglomeration, as can be observed for the sample with 30% strontium treated at 700 °C.

The morphology of $\text{La}_{0.85}\text{Sr}_{0.15}\text{MnO}_3$ and $\text{La}_{0.70}\text{Sr}_{0.30}\text{MnO}_3$ powders heat-treated at 450 and 950 °C is illustrated in the SEM micrographs of Figures 10 to 13. These micrographs confirmed the powder agglomeration. Such agglomerates formation can be reduced, adopting lower heat treatment temperatures and also by means of more efficient milling and de-agglomeration processes after the heat treatment, which should improve the size homogeneity of the sintered samples.

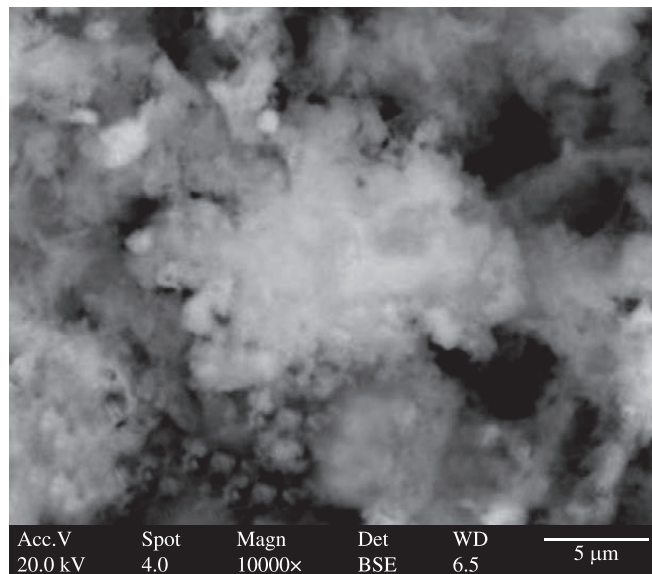


Figure 13. SEM micrograph of $\text{La}_{0.67}\text{Sr}_{0.33}\text{MnO}_3$ calcined at 950 °C/4 hours.

4. Conclusions

The synthesis by the polymeric precursor method proved to be adequate for the production of $\text{La}_{1-x}\text{Sr}_x\text{MnO}_3$ powder oxides, with a formed perovskite structure starting from 600 °C. These powders show a low crystallite sizes and also relatively high specific surface areas. The nanocrystallite sizes of the powders ranged between 17 to 35 nm. It can be noted that the average crystallite sizes obtained for LSM perovskite-type oxides containing the intermediate 0.22% Sr showed a tendency for decreasing crystallite size and increasing specific surface area.

Acknowledgements

The authors gratefully acknowledge the financial support of the Brazilian Research Funding Institutions ANP (2001.6956-0), FAPERN (300266/2004-9) and FAPESPA (025/2008).

References

- Capon F, Horwat D, Pierson JF, Chapusot V and Billard A. Strontium-doped lanthanum manganite coatings crystallised after air annealing of amorphous co-sputtered films. *Materials Chemistry and Physics*. 2009; 116:219-222.
- Smith JR, Chen A, Gostovic D, Hickey D, Kundinger D, Duncan KL et al. Evaluation of the relationship between cathode microstructure and electrochemical behavior for SOFCs. *Solid State Ionics*. 2009; 180:90-98.
- Chen X, Zhen Y, Li J and Jiang SP. Chromium deposition and poisoning in dry and humidified air at $(\text{La}_{0.8}\text{Sr}_{0.2})_{0.9}\text{MnO}_{3+\delta}$ cathodes of solid oxide fuel cells. *International Journal of Hydrogen Energy*. 2010; 35:2477-2485.
- Yang J, Muroyama H, Matsui T and Eguchi K. A comparative study on polarization behavior of $(\text{La,Sr})\text{MnO}_3$ and $(\text{La,Sr})\text{CoO}_3$ cathodes for solid oxide fuel cells. *International Journal of Hydrogen Energy*. 2010; 35:10505-10512.
- Genchu T., Yun Y., Wei C. and Yunzhen C. The electrical resistivity and thermal infrared properties of $\text{La}_{1-x}\text{Sr}_x\text{MnO}_3$ compounds. *Journal of Alloys and Compounds*. 2008; 461:486-489.
- Tang G, Yu Y, Chen W and Cao Y. The electrical resistivity and thermal infrared properties of $\text{La}_{1-x}\text{Sr}_x\text{MnO}_3$ compounds. *Journal of Alloys and Compounds*. 2008; 461:486-489.
- Budak S, Özdemir M and Aktas B. Temperature dependence of magnetic properties of $\text{La}_{0.67}\text{Sr}_{0.33}\text{MnO}_3$ compound by ferromagnetic resonance technique. *Physica B*. 2003; 339:45-50.
- Yang W-D, Huang S-H and Chang Y-H. Microstructure, magnetoresistance and electrical properties of $\text{La}_{0.67}\text{Sr}_{0.33}\text{MnO}_3$ films synthesized from citric acid and ethylene glycol. *Thin Solid Films*. 2005; 478:42-48.
- Sakthipandi K, Rajendran V, Jayakumar T, Raj B and Kulandivelu P. Synthesis and on-line ultrasonic characterisation of bulk and nanocrystalline $\text{La}_{0.68}\text{Sr}_{0.32}\text{MnO}_3$ perovskite manganite. *Journal of Alloys and Compounds*. 2011; 509:3457-3467.
- Fleig J. Solid oxide fuel cell cathodes: polarization mechanisms and modeling of the electrochemical performance. *Annual Review of Materials Research*. 2003; 33:361-382.
- Matsuzaki Y and Yasuda I. Electrochemical properties of reduced-temperature SOFCs with mixed ionic–electronic conductors in electrodes and/or interlayers. *Solid State Ionics*. 2002; 152-153:463–468.
- Berenov AV, MacManus-Driscoll JL and Kilner JA. Oxygen tracer diffusion in undoped lanthanum manganite. *Solid State Ionics*. 1999; 122:41-49.
- Gupta RK, Kim EY, Kim YH and Whang CM. Effect of strontium ion doping on structural, thermal, morphological and electrical properties of a co-doped lanthanum manganite system. *Journal of Alloys and Compounds*. 2010; 490:56-61.
- Souza S, Visco SJ, De Jonghe LC. Thin-film solid oxide fuel cell with high performance at low temperature. *Solid State Ionics*. 1997; 98:57-61.
- Sahu AK, Ghosh A, Suri AK. Characterization of porous lanthanum strontium manganite (LSM) and development of yttria stabilized zirconia (YSZ) coating. *Ceramics International*. 2009; 35:2493-2497.
- Hamedani HA, Dahmen K-H, Li D, Peydaye-Saheli H, Garmestani H and Khaleel M. Fabrication of gradient porous LSM cathode by optimizing deposition parameters in ultrasonic spray pyrolysis. *Materials Science and Engineering B*. 2008; 153:1-9.
- Chen K, Lü Z, Chen X, Ai N, Huang X, Du X et al. Development of LSM-based cathodes for solid oxide fuel cells based on YSZ films. *Journal of Power Sources*. 2007; 172:742-748.
- Silva WJ, Melo DMA, Soares SFCX, Pimentel PM, Nascimento RM, Martinelli AE. et al. Síntese de manganita de lantânio com substituição parcial do La por Sr pelo método citrato. *Revista Matéria*. 2007; 12(1):65-71.
- Bidrawn F, Kim G, Aramrueang N, Vohs JM, Gorte RJ. Dopants to enhance SOFC cathodes based on Sr-doped LaFeO_3 and LaMnO_3 . *Journal of Power Sources*. 2010; 195:720-728.
- Giraud S and Canel J. Young's modulus of some SOFCs materials as a function of temperature. *Journal of the European Ceramic Society*. 2008; 28:77-83.
- Pechini M. Method of preparing lead and alkaline earth titanates and niobates and coating methods using the same to form a capacitor. 1967. U. S. Pat. Number 3.330.697.
- Yang W-D, Chang Y-H and Huang S-H. Influence of molar ratio of citric acid to metal ions on preparation of $\text{La}_{0.67}\text{Sr}_{0.33}\text{MnO}_3$ materials via polymerizable complex process. *Journal of the European Ceramic Society*. 2005; 25:3611-3618.
- Conceição L, Silva CRB, Ribeiro NFP and Souza MMVM. Influence of the synthesis method on the porosity, microstructure and electrical properties of $\text{La}_{0.7}\text{Sr}_{0.3}\text{MnO}_3$ cathode materials. *Materials Characterization*. 2009; 60:1417-1423.
- Kakihana M, Arima M, Yoshimura M, Ikeda N and Sugitani Y. Synthesis of high surface area $\text{LaMnO}_{3+\delta}$ by a polymerizable complex method. *Journal of Alloys and Compounds*. 1999; 283(1-2):102-105.
- Berger D, Fruth V, Jitaru I and Schoonman J. Synthesis and characterisation of $\text{La}_{1-x}\text{Sr}_x\text{CoO}_3$ with large surface area. *Materials Letters*. 2004; 58(19):2418-2422.
- Fritsch SG, Alphonse P, Calmet C, Coradin H, Pailhades P and Rousset A. Du choix du précurseur pour la synthèse de poudres d'oxydes $\text{La}_{1-x}\text{Sr}_x\text{MnO}_3$. *Comptes Rendus Chimie*. 2005; 8(2):219-227.
- Barret EP, Joyner LG and Halenda PH. The determination of pore volume and area distribution in porous solids. I: computation from nitrogen isotherms. *Journal of the American Chemical Society*. 1951; 73:373-380.
- Nakamoto K. *Infrared and raman spectra of inorganic and coordination compounds*. 3rd ed. New York: John Wiley & Sons, 1978.
- Liou Y-C. Effect of strontium content on microstructure in $(\text{La}_x\text{Sr}_{1-x})\text{FeO}_3$ ceramics. *Ceramics International*. 2004; 30(5):667-669.
- Berger D, Fruth V, Jitaru I and Schoonman J. Synthesis and characterisation of $\text{La}_{1-x}\text{Sr}_x\text{CoO}_3$ with large surface area. *Materials Letters*. 2004; 58(19):2418-2422.
- Shannon RD. Revised effective ionic radii and systematic studies of interatomic distances in halides and chalcogenides. *Acta Crystallographica*. 1976; A32:751-767.